Environ. Sci. Technol. **2010,** *44,* 6054–6061

Characteristics of Lead Corrosion Scales Formed during Drinking Water Distribution and Their Potential Influence on the Release of Lead and Other Contaminants

EUN JUNG KIM AND JOSE E. HERRERA*

Department of Civil and Environmental Engineering, University of Western Ontario, London, Ontario Canada, N6A 5B9

Received October 26, 2009. Revised manuscript received June 24, 2010. Accepted July 7, 2010.

Destabilization of the corrosion scale present in lead pipes used in drinking water distribution systems is currently considered a major problem for municipalities serviced in part by lead pipes. Although several lead corrosion strategies have been deployed with success, a clear understanding of the chemistry of corrosion products present in the scale is needed for an effective lead control. This contribution focuses on a comprehensive characterization of the layers present in the corrosion scale formed on the inner surfaces of lead pipes used in the drinking water distribution system of the City on London, ON, Canada. Solid corrosion products were characterized using X-ray diffraction (XRD), Raman spectroscopy, Fourier transform infrared (FTIR) spectroscopy, and X-ray photoelectron spectroscopy (XPS). Toxic elements accumulated in the corrosion scale were also identified using inductively coupled plasma (ICP) spectrometry after acid digestion. Based on the XRD results, hydrocerussite was identified as the major lead crystalline corrosion phase in most of the pipes sampled, while cerussite was observed as the main crystalline component only in a few cases. Lead oxides including PbO_2 and Pb_3O_4 were also observed in the inner layers of the corrosion scale. The presence of these highly oxidized lead species is rationalized in terms of the lead(II) carbonate phase transforming into lead(IV) oxide through an intermediate Pb_3O_4 ($2Pb^{II}O \cdot Pb^{IV}O_2$) phase. In addition to lead corrosion products, an amorphous aluminosilicate phase was also identified in the corrosion scale. Its concentration is particularly high at the outer surface layers. Accumulation of toxic contaminants such as As, V, Sb, Cu, and Cr was observed in the corrosion scales, together with a strong correlation between arsenic accumulation and aluminum concentration.

Introduction

Lead is a toxic heavy metal and human exposure to elevated concentrations of lead in drinking water poses significant health risks such as adverse impact on nervous and reproductive systems (*1*). Lead is mainly introduced to drinking water through corrosion of lead bearing plumbing materials. Leaching of lead from plumbing materials can occur due to different circumstances, including the age of lead bearing materials, kinetic, and thermodynamic stability of the inner scale formed in the lead pipe, and water quality characteristics (*2*). In general, lead passivation occurs over time by the formation of corrosion products such as cerussite ($PbCO_3$), hydrocerussite ($Pb_3(CO_3)_2(OH)_2$), plumbonacrite ($Pb_{10}(CO_3)_6(OH)_6O$), litharge (PbO), and plattnerite (PbO_2) on the inner walls of the pipe. The formation of this passivating scale lowers the amount of lead leached to water running through the pipe (*2*). However, the stability of this scale strongly depends on the quality of the water running through the pipes, which can induce chemical transformations and dissolution of corrosion products in the form of aqueous ionic species of lead, and/or release of particulate and colloidal lead-containing solids into the aqueous phase. Destabilization of the scale results in high concentrations of lead in drinking water and can also potentially release toxic elements accumulated in the corrosion scale.

Lead levels above drinking water standards were found in drinking water in Washington, DC.and Greensville, NC in 2003 and 2005, respectively. These incidents are now known to be caused by a change in water quality when chloramines began to be used as disinfectant instead of chlorine (*3*). This change lowered the redox potential of the aqueous phase, causing the destabilization and dissolution of PbO_2 present in the lead scale. In London, ON, Canada, lead concentrations in about 25% of sampled tap water exceeded the water quality standard, 10 μg/L, up to 65 μg/L in the spring of 2007 (*4*). These unusually high lead levels are believed to be caused by the lower pH levels that resulted from the addition of acidified alum since the early 1990s. A detailed description of London's water distribution system and the major water quality parameters of the treated water are summarized in the Supporting Information (SI) (Table S1 and Figure S1).

Currently, very little is known about the chemistry of the corrosion products present inside the lead plumbing materials used for drinking water distribution in London. Moreover, whether these changes in pH have destabilized the lead scale present in the pipes is still unclear. Therefore, a comprehensive understanding of the chemistry of corrosion products present in the scale is essential to assess the stability of the lead scale, to forecast the effects of future changes in water treatment, and to develop an effective corrosion control program. This study reports the results of a comprehensive characterization of the corrosion scales formed on the inner surfaces of lead pipes used in the drinking water distribution system of the City of London. Solid corrosion products were investigated using X-ray diffraction (XRD), Raman spectroscopy, Fourier transform infrared (FTIR) spectroscopy, and X-ray photoelectron spectroscopy (XPS). Toxic and common elements accumulated in the corrosion scale were analyzed by inductively coupled plasma (ICP) spectrometry after acid digestion.

Experimental Section

Lead pipe samples were obtained as a part of the Lead Service Replacement Program put in place by the City of London, ON, Canada. These pipes were reclaimed from March to May 2009. These pipes were originally installed from 1880 to 1947 and have been used for domestic drinking water distribution until the time they were removed for replacement. The list of pipe samples used in this study and their characteristics are summarized in Table 1. The pipes were cut longitudinally and corrosion scale solids were harvested using stainless steel spatulas. Among these samples, pipe 3, installed in 1880,

* Corresponding author phone: 1-519-661-2111x81262; fax: 1-519-661-3498; e-mail: jherrera@eng.uwo.ca.

10.1021/es101328u
Published on Web 07/19/2010

TABLE 1. List of Lead Pipe Samples and Summary of Main Solid Phases Observed by XRD, Raman, and FTIR Studies

sample	year of installation	sampling	main phases present in the corrosion scale
P1	unknown	03/16/09−03/20/09	$Pb_3(CO_3)_2(OH)_2$[a], $PbCO_3$, PbO_2, PbO, aluminum silicate
P2	unknown	03/16/09−03/20/09	$PbCO_3$[a], $Pb_3(CO_3)_2(OH)_2$, PbO_2, aluminum silicate
P3	1880	04/15/09	$Pb_3(CO_3)_2(OH)_2$[a], $PbCO_3$, PbO_2, Pb_3O_4, aluminum silicate
P4	1899	05/07/2009	$Pb_3(CO_3)_2(OH)_2$[a], $PbCO_3$, PbO_2, aluminum silicate
P5	1905	05/15/09	$Pb_3(CO_3)_2(OH)_2$[a], $PbCO_3$, PbO, PbO_2, aluminum silicate
P6	1905	05/15/09	$Pb_3(CO_3)_2(OH)_2$[a], $PbCO_3$, PbO_2, aluminum silicate
P7	1905	05/15/09	$Pb_3(CO_3)_2(OH)_2$[a], $PbCO_3$, PbO_2, aluminum silicate
P8	1908	05/19/09	$PbCO_3$[a], $Pb_3(CO_3)_2(OH)_2$,PbO, PbO_2, aluminum silicate
P9	1919	05/14/09	$PbCO_3$[a], $Pb_3(CO_3)_2(OH)_2$, Pb_3O_4, PbO_2, aluminum silicate
P10	1927	04/15/09	$Pb_3(CO_3)_2(OH)_2$[a], $PbCO_3$, Pb_3O_4, aluminum silicate
P11	1947	05/14/09	$Pb_3(CO_3)_2(OH)_2$[a],PbO, PbO_2, aluminum silicate

[a] Major crystalline phase observed by XRD.

(P3, Table 1) was the oldest in our study. This sample showed distinctly layers of different colors and textures (SI Figure S2). The outermost layer (L1) was rusty brown in color and covering approximately 30% of the entire surface of the corrosion scale. This layer was easily separated from the inner layers, which indicates this layer can be easily disturbed by physical impact such as an unusually high water flow rate. Underneath the outermost layer, L1, an orange color layer was present covering most of the surface, this was separately harvested and labeled as L2. A yellowish color layer (L3) was observed under the aforementioned orange color layer (L2). Underneath the yellow layer, a thin dark brown color layer was found, covering the entire surface of the metallic lead pipe. This layer was strongly adhered to the entire inner surface of the lead pipe. The thin dark brown innermost layer, L4, was harvested with caution to avoid damaging to the surface of the lead pipe. Each layer was carefully harvested separately and four layers (samples L1, L2, L3, and L4) were identified in the pipe, where L1 was the outermost layer furthest away from the pipe surface and L4 was the innermost layer contacting with pipe surface. We should mention that some overlap between adjacent layers was inevitable during layer harvest. Since the surface coverage by each layer in the pipe was not uniform, we were unable to perform an exact quantification of the individual contributions of each layer to the corrosion scale. The overall thickness of the corrosion scale was roughly 1 mm. Based on the weight of each layer we obtained we can state that the L3 layer accounted for almost 70% of the total corrosion scale mass. Layers L1 and L2 contributed with more than 10% each, while layer L4 contributed to roughly 5% to the total corrosion scale mass. Each layer was separately studied except for the case of elemental analysis. These harvested solid samples were stored in a desiccator until analysis.

All solids were analyzed by XRD, Raman spectroscopy, FTIR spectroscopy, and ICP spectrometry after acid digestion. Selected samples were analyzed by XPS and scanning electron microscopy (SEM). The XRD data were collected on a Rigaku-Miniflex powder diffractometer using Cu K-α ($\lambda = 1.54059$ Å) radiation obtained at 30 kV and 15 mA. Scans were taken over the range of 10−90° 2θ with 0.05° step size. The absorbance spectra of corrosion scales in the middle IR (400−4000 cm^{-1}) were obtained using a Bruker Vector 22 FTIR spectrometer using an ATR cell. The surface chemical composition and detailed oxidation state of the elements present on the scale was characterized using a Kratos Axis Ultra X-ray photoelectron spectroscopy (XPS) with monochromatic Al K-α X-rays. Broad scans were obtained using 160 eV pass energy, while narrow high resolution scans were obtained using 20 eV pass energy. The charge effect was corrected using the C 1s line at 284.8 eV. The obtained spectra were fitted using CasaXPS. Raman analysis was performed using a Renishaw model 2000 Raman spectrometer equipped with a 633 nm laser. The samples were analyzed in macro mode using a 20× long working length objective and 1.65 mW laser intensity. A number of areas on each sample were analyzed and the Raman data were compared with the Raman spectra of reference lead compounds (Sigma-Aldrich) (SI Figure S4). SEM analysis was performed using a LEO/Zeiss 1540XB FIB/SEM. For elemental analysis, 0.5−1 g of solid sample was weighed and digested using U.S. EPA Method 3050B (*5*). These acid digested samples were quantitatively analyzed using an ICP-OES (Varian, Inc., Vista-Pro Axial).

Results and Discussion

Major solid phases present in the corrosion scales of lead pipes observed by XRD, Raman, and FTIR are summarized in Table 1. The X-ray diffraction patterns indicate that lead carbonates (hydrocerussite and cerussite) are the major crystalline phases of the corrosion scales of lead pipes, whereas lead oxides such as plattnerite and litharge are observed in some cases. Among all these, hydrocerussite is the main crystalline component for most of the samples, except for samples P2, P8, and P9 where cerussite was identified as the main crystalline phase by XRD.

Composition of Layered Scales: XRD and Raman. XRD results for the four layered corrosion scales harvested from the oldest pipe (P3) are shown in Figure 1. The XRD pattern of the outermost layer, L1, did not show any clear diffraction peak, indicating the presence of poorly crystalline phases. The XRD of the remaining layers (L2−L4) indicate the presence of hydrocerussite as the major crystalline lead phase. A small amount of cerussite was also observed in these samples. On the other hand, plattnerite (PbO_2) was observed along with hydrocerussite in the innermost layer, closest to the pipe surface (L4). The Raman spectra for these samples are shown in Figure 2. Here the outermost layer, L1, showed strong bands at 139 cm^{-1} and 1049 cm^{-1}, which are associated with PbO_2 and hydrocerussite, respectively (Figure 2a, SI Figure S4). The XRD and Raman results clearly indicate that amorphous forms of PbO_2 and hydrocerussite phases are present on the outermost layer (L1) of the corrosion scale. A broad band centered at around 650 cm^{-1} was also observed on this sample. This band is attributed to the bending mode of an Al−O−Si moiety (Figure 2b) (*6, 7*), suggesting the presence of an amorphous aluminosilicate phase. This was confirmed using FTIR spectroscopy (see discussion below). In agreement with the XRD results, the Raman spectra obtained on the inner layers of the scale (L2−L4) indicate that hydrocerussite is the main species present on these samples and that PbO_2 is present in the innermost layer (L4) (Figure 2c). A rather broad band at around 540 cm^{-1} was also observed for the inner layer samples (L3 and L4), which suggests the presence of minium (Pb_3O_4) (Figure 2d, SI Figures

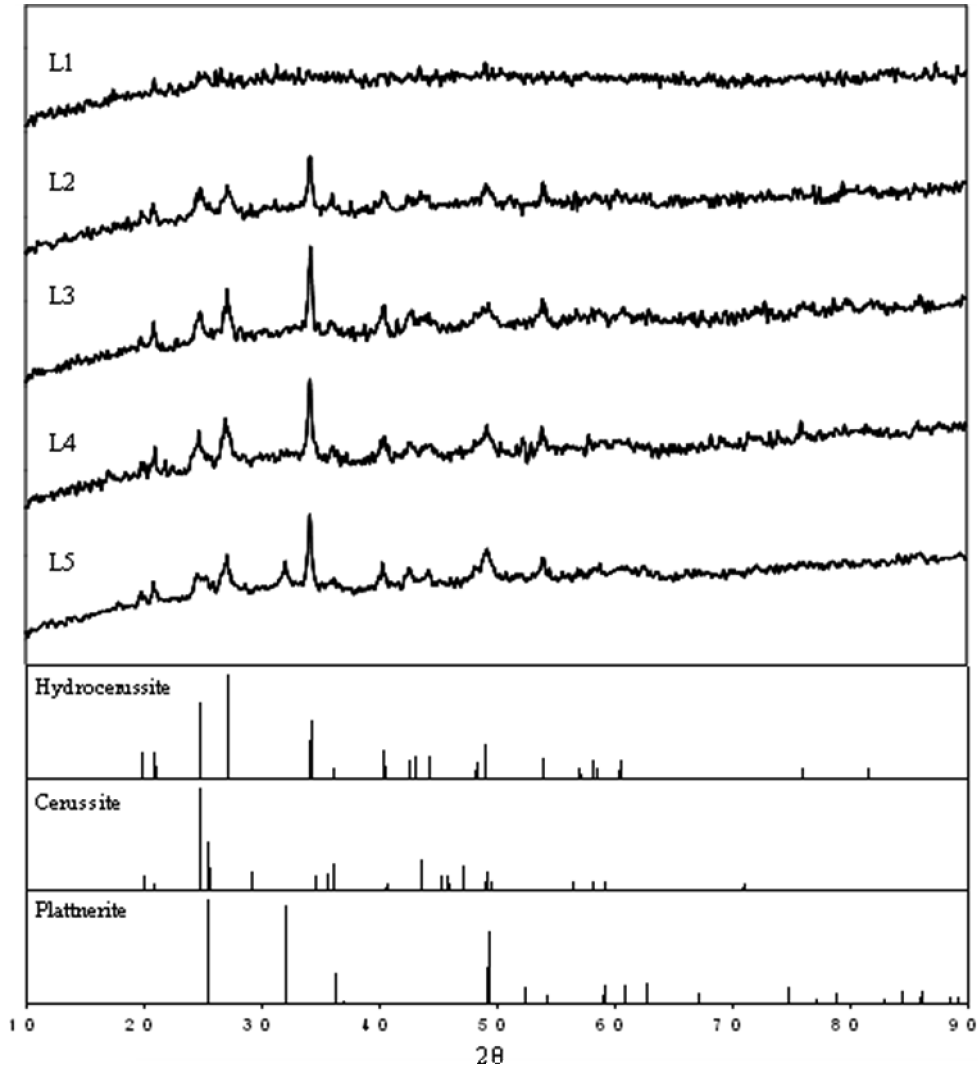

FIGURE 1. X-ray diffraction patterns obtained on the corrosion scale layers L1 (outermost layer) to L4 (innermost layer) harvested from lead pipe sample P3.

S4−S5) (*8*). It is well-known that PbO_2 is a highly insoluble lead component, and its presence is considered to be beneficial for corrosion control in lead plumbing water distribution systems (*9*). However, PbO_2 can be only formed at highly oxidative conditions such as those in chlorinated water (*9*). Although PbO_2 has been previously observed in the form of a very thin surface layer at the water/corrosion scale interface (*10*), our data clearly indicate the presence of PbO_2 in the inner corrosion scale layer (L4) as well as in the surface layer.

We further studied the morphology of each scale layer using SEM (SI Figure S7). All layers showed very fine aggregated particles (<50 nm). The innermost layer (L4) is a thin and adherent film that covers the entire inner pipe surface. The SEM image indicated that this innermost layer had a more densely aggregated structure. In contrast, the outer layers were thick, porous, and rather loosely attached. Similar electron microscopy studies have been carried out on lead corrosion solids although on most of cases pure crystalline phases were analyzed (*11*−*13*).

Based on the SEM observations, we propose that at the early stages of lead corrosion, lead was rapidly oxidized to form a compact, adherent film that covered the entire inner surface of the pipe. The well water used in the early years of the last century in the distribution system had high alkalinity and relatively high pH (pH ∼ 8). Under these conditions, it is well-known that the formation of hydrocerussite is favorable (*14*). After hydrocerussite was formed, some of it was further oxidized to form PbO_2 under the highly oxidative conditions that resulted from the aggressive chlorination process implemented in 1915 (*4*). In fact, Pb(IV) oxides (scrutinyite (α-PbO_2) and plattnerite (β-PbO_2)) have been reported to form from Pb(II) precursor mineral phases (cerussite and hydrocerussite) in chlorinated water (*9, 12*); particularly taking into consideration that groundwater has conditions that enable the persistence of free chlorine (*9*). Overtime, an outer corrosion layer developed over the tight adherent layer, which is porous and loosely attached. These porous outer layers are mainly composed of hydrocerussite and small amounts of cerussite. It is likely that the formation and transformation of lead species present in the corrosion scales were affected by change of water quality over time due to the changes in water source (ground vs surface) and water treatment procedure. Particularly, for the case when water source was shifted from groundwater to surface water. This change on water quality affected the morphology of the corrosion scale.

The XRD study of the innermost layer indicated the presence of Pb(IV) oxide. But only plattnerite was observed and scrutinyite was not detected. It has been proposed that scrutinyite is more thermodynamically stable than plattnerite and that scrutinyite is the final oxidation product of hydrocerussite (*9*). This transformation occurs as follows: hydrocerussite → cerussite → plattnerite → scrutinyite (*9*). Thus

the observation of only plattnerite in the corrosion scale indicates that the oxidation of hydrocerussite has not reached yet the final product (scrutinyite) or that the reverse reaction has taken place. Pb(IV) oxides can also be reversely transformed to Pb(II) phases at lower redox potentials. Indeed, Lytle and Shock have reported that Pb(IV) oxides are reversely transformed to $PbCO_3$ when chlorine is consumed to depletion (*9*). The observation of amorphous phase of Pb(IV) oxide at the outermost layer suggests current and recent water quality conditions have both favorable conditions for PbO_2 formation.

Our XRD and Raman results indicate that a minium (Pb_3O_4) phase is present in the L3 and L4 layers. Little is known about the redox interconversion of Pb(II) and Pb(IV) at the typical conditions present in of drinking water, although Pb(III) intermediate products have been observed in the electrochemical oxidation of Pb(II) to Pb(IV) (*15*). Based on our results, we can hypothesize that Pb_3O_4 is an intermediate product of the redox transformation between Pb(II) and Pb(IV) phases. In addition, it has been reported that hydrocerussite is first transformed to cerussite before it is oxidized to PbO_2 by chlorine (*9, 12*), which could explain the presence of the small amount of cerussite observed in the corrosion scale. The overall reactions that lead to the lead oxidation products identified in the scale can be hypothesized as follows:

$$Pb(s) + 1/2O_2 + H_2O \leftrightarrows Pb^{2+} + 2OH^- \quad (1)$$

$$3Pb^{2+} + 2CO_3^{2-} + 2OH^- \leftrightarrows Pb_3(CO_3)_2(OH)_2 \quad (2)$$

$$Pb_3(CO_3)_2(OH)_2 + H_2CO_2 \leftrightarrows 3PbCO_3 + 2H_2O \quad (3)$$

$$3PbCO_3 + HOCl + 3H_2O \leftrightarrows Pb_3O_4 + HCl + 3H_2CO_3 \quad (4)$$

$$Pb_3O_4 + 2HOCl \leftrightarrows 3PbO_2 + 2HCl \quad (5)$$

Composition of Layered Scales: FTIR and XPS. Figure 3 shows the infrared spectra obtained for the four layered corrosion scales together with spectra of pure hydrocerussite and a synthesized allophone like aluminosilicate phase. All spectra of corrosion layers show strong bands centered at 1400 and 681 cm^{-1}, which are characteristic for hydrocerussite. All corrosion layers also exhibit a band near 950 cm^{-1}, which is characteristic band of aluminosilicate. This band is a typical of a Si−O−Al stretching vibration and characteristic of aluminosilicates such as imogolite or Al rich allophane (Si/Al <1) (*16*−*19*). The strong band between 700 and 500 cm^{-1} can be attributed to Al−O and Al−OH bonds (*19*). Surface analysis by XPS shows that Si/Al atomic ratio is consistently close to 0.3 for all layers except for the innermost one, L4 (SI Table S2). This confirms that the corrosion scales contain an Al rich aluminosilicate phase. Moreover, the intensities of the observed Si−O−Al and Al−O/Al−OH

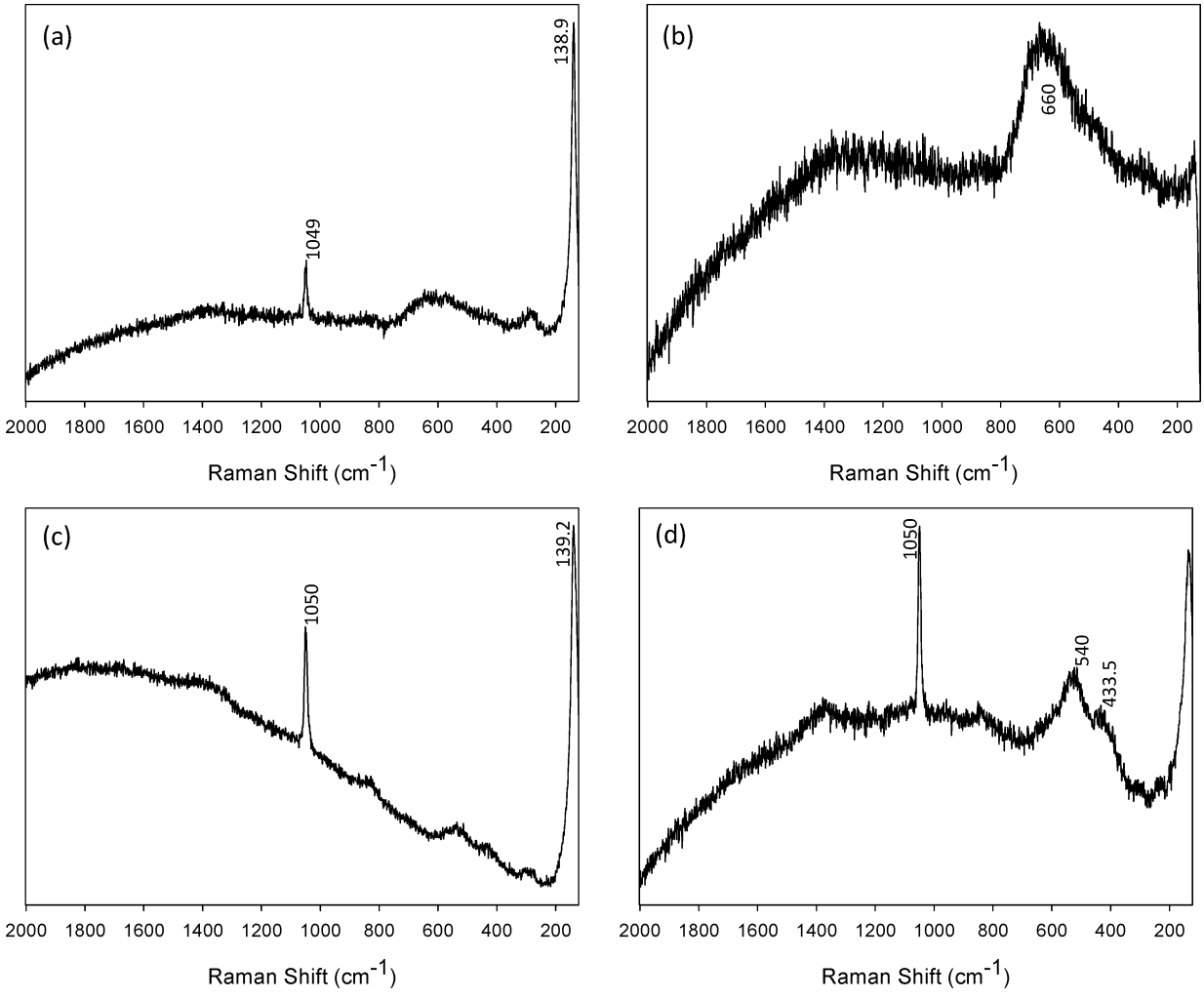

FIGURE 2. Raman spectra obtained for the corrosion scale layers harvested from lead pipe sample P3. (a) and (b): two different sample areas of the outermost layer L1, (c) and (d): two different sample areas of the innermost layer L4.

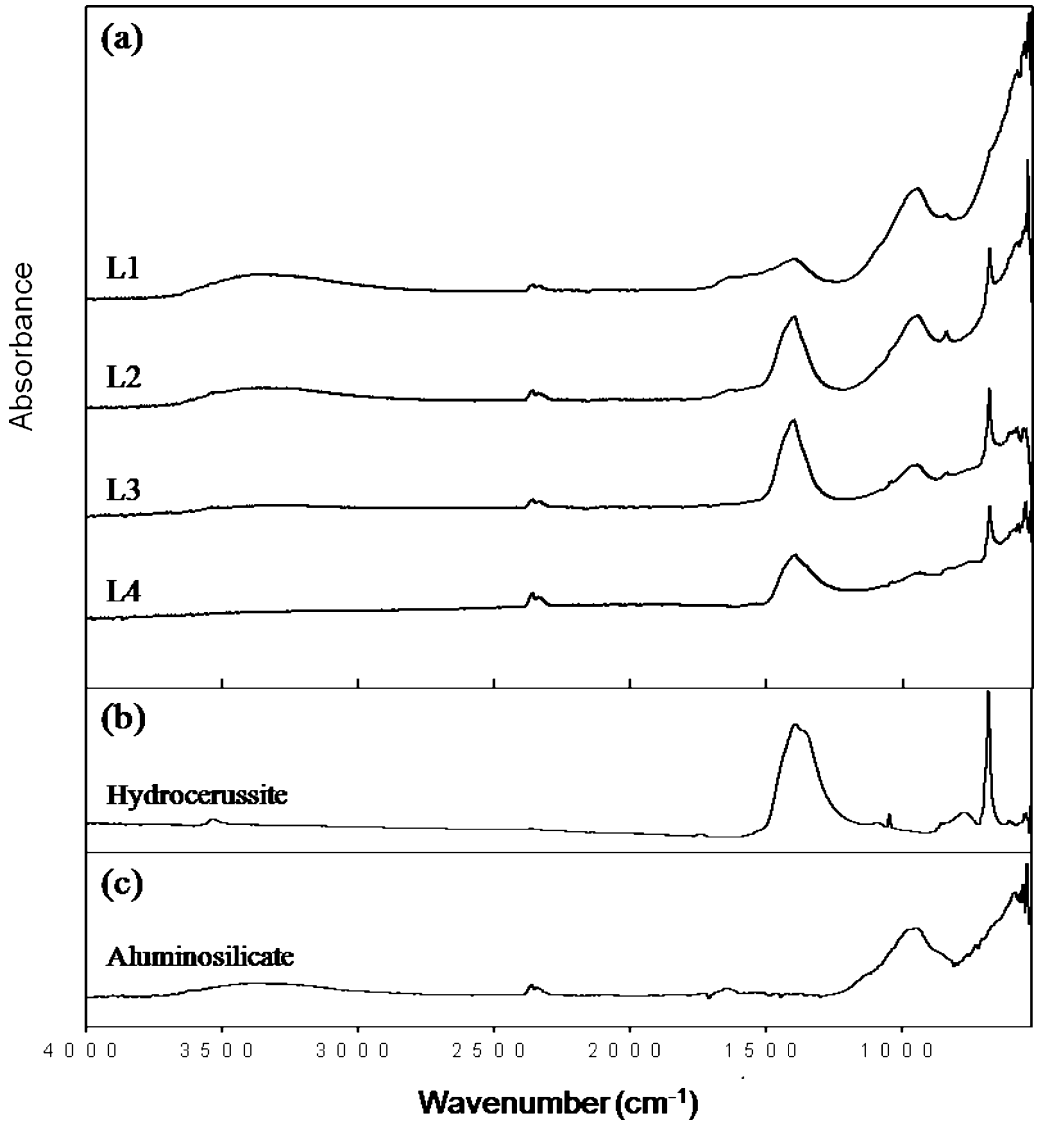

FIGURE 3. FTIR absorbance spectra obtained on (a) the corrosion scale layers L1 (outermost layer) to L4 (innermost layer) harvested from lead pipe P3, (b) pure hydrocerussite and (c) synthesized allophone like aluminosilicate (Si/Al molar ratio 0.67).

infrared bands are stronger in the outer layers than in inner layers. This reflects the fact that the aqueous phase acts as source of the aluminosilicate phase. The first top two layers, L1 and L2, also show prominent water bands near 3500 and 1640 cm^{-1} due to the OH stretching and HOH bending vibrations, respectively (*18*), which could indicate the presence of a hydrated aluminosillicate phase on the surface layer.

The FTIR results indicate that a hydrated aluminosilicate of low Si/Al ratio is present and mixed with hydrocerussite. Aluminosilicate was not observed on the XRD diffractograms on these samples since they are known to yield very poor resolved X-ray diffractograms due to diffuse scattering (*16*). This points out to the presence of an amorphous form of aluminosilicate in the corrosion scale. Aluminosilicate is known to form by the reaction between Al^{3+} ions (byproduct of the alum used as coagulant during water potabilization process) and naturally occurring silica particles present in water (*20*). Indeed, aluminum containing scales are commonly observed in water distribution systems (*20*). The City of London has used alum since 1967 as a coagulant during its water treatment at relatively high concentrations before the application of acidified alum in early 1990s; leading to high aluminum concentrations in the water that entered the distribution system in the past. Additionally, the City of London's water quality data in 2007 and 2008 indicate that the concentration of silica in treated water was around 1.4−1.6 mg/L (SI Table S1). These conditions seem favorable to the formation of an aluminosilicate phase. To verify this hypothesis, we input the values reported for the concentrations of aluminum and silica in the City of London's treated water the system into a Visual MINTEQ (ver. 2.61) simulation (*21*). The results showed that under these conditions the system is supersaturated with imogolite. In principle, this aluminosilicate phase could provide a corrosion protective barrier in the water distribution pipes and/or adsorb trace metals present in water. However, it is not certain at this point how these aluminosilicate deposits affect the concentration of lead in drinking water (*20*).

The surface composition in atomic percent ratios of the layered corrosion scales determined by XPS broad scans is shown in SI Table S2. The surfaces of the corrosion scales are mainly composed of Pb, O, C, Al, Si, and Fe. The outer scale layers show a lower lead, carbon, and chlorine concentration with higher concentrations of oxygen, aluminum, silicon, iron, and calcium; whereas inner scale layers show the opposite. A clear trend is observed for the case of aluminum and lead: the concentration of lead is increasing and aluminum is decreasing as we approach the layers in closest contact with the pipe surface. Figure 4 presents the

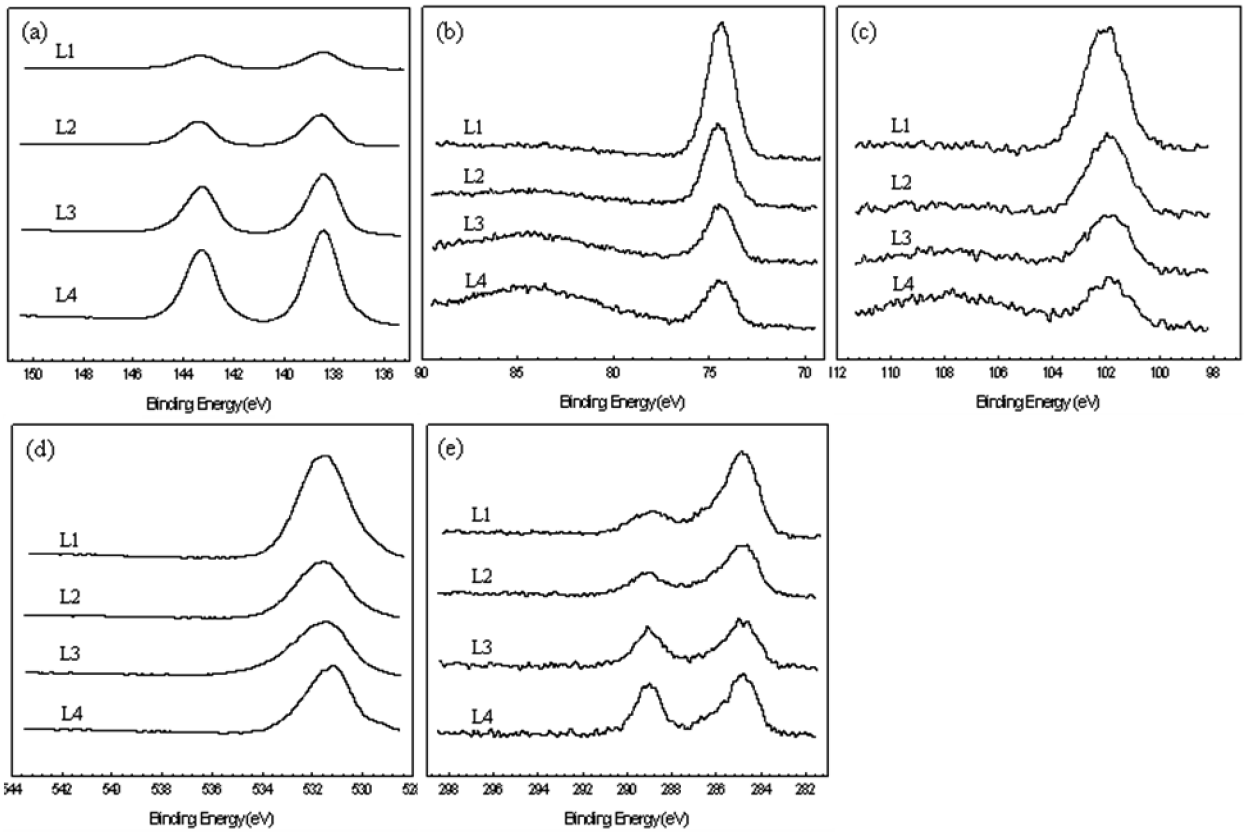

FIGURE 4. XPS spectra obtained for the (a) Pb 4f, (b) Al 2p, (c) Si 2p, (d) O 1s, and (e) C 1s lines on each corrosion layer harvested from lead pipe sample P3.

XPS narrow scan spectra for the Pb 4f, Al 2p, Si 2p, O 1s, and C 1s lines obtained on the layered corrosion scales (L1−L4). The Pb 4f spectra show two main peaks at around 138 eV (Pb $4f_{7/2}$) and 143.5 eV (Pb $4f_{5/2}$). The Pb $4f_{7/2}$ data were fitted using two component set of peaks, one with its main band at around 138.5 eV and the other one at 137 eV. The results of this fitting are shown in SI Table S3. The main contribution for the fitting comes from the peak centered at 138.5 eV, which corresponds to hydrocerussite (SI Figure S10). The contribution of the peak at 137 eV, attributed to PbO_2, becomes only relevant to the outermost layer L1 sample and innermost layers, L4. These results are consistent with the XRD and Raman results. The Al 2p line shows its peak centered around 74.4 eV, which is typical of aluminosilicate compounds (*22*). For the case of silicon, the Si 2p spectra shows a peak centered at around 102 eV, which has been previously assigned to Al−O−Si bonds (*23*). In agreement with the FTIR results, the XPS Al 2p and Si 2p spectra indicate the presence of aluminosilicate on the surface of the corrosion scales. For the case of oxygen, the O 1s spectra shows a shift on the peak position to lower binding energies as the layers become closer to the pipe surface. This suggests that there is an increase in the oxygen linked to lead carbonate (~531.1 eV) at the expense of aluminosilicate (~531.9 eV) decrease as we move closer to the pipe surface further away from the water phase (*24*). A similar trend is observed for the C1s spectra. For this case two main peaks are observed, one at around 285 eV and other at 289 eV. The peak centered at 289 eV is assigned to CO_3^{2-} in lead carbonate phases (*25*). The peak intensity increases for the inner layers, indicating the increase in concentration of this phase.

Accumulation of Contaminants in the Corrosion Scale. Elemental chemical analysis indicated that the major metallic elements accumulated in the corrosion scales (besides lead) were Al, Fe, Mn, and Ca (Table 2). Among these, Al was the most abundant in all the samples. Presence of toxic contaminants such as As, V, Sb, Cu, and Cr was also observed with average concentrations of 128, 802, 119, 556, and 47 mg/kg, respectively. The average concentration of accumulated As (128 mg/kg) in the City of London pipes is higher than average (87 mg/kg) reported for U.S. lead pipe scales (*26*), but lower than accumulated concentrations observed for scales present on iron pipes (*27*).

The accumulation of these contaminants in the pipe corrosion scale can be affected by the quality of the water running through the pipes, pipe morphology, and composition of the corrosion scale phase. Oxides of iron, aluminum, and manganese are known to be the major minerals controlling arsenic speciation in aquifers (*28*). In our case a strong correlation was observed between arsenic and aluminum concentrations (Figure 5, SI Table S4). This suggests that the aluminosilicate phase in the corrosion scale affects the accumulation of arsenic. Previous studies have reported that poorly crystalline aluminosilicate minerals play an important role in regulating metal concentrations in the environment, due to their high specific surface areas and surface reactivity (*18, 29*). Arsenic adsorption onto amorphous aluminosilicate (allophone) was reported to occur by ligand exchange reactions between arsenate and surface coordinated water molecules and hydroxyl and silicate ions at near neutral pH (*29*). Therefore, it is likely that the aluminosilicate phase present in the corrosion scale adsorbs arsenic, leading to arsenic accumulation in the pipe scale.

Environmental Implications. The formation and transformation of the corrosion products identified in this study are influenced by various factors including water quality and pipe morphology. While it is expected that corrosion products observed on different water distribution systems will be quite different depending on water sources and different water treatment methods, our study, focused on samples obtained from a single water distribution system, indicates that the composition of corrosion products is also subject to these

TABLE 2. Concentrations of Contaminants Accumulated in the Corrosion Scales of Lead Pipes (mg/kg or wt% as Indicated)

	Al	As	Ba	Ca	Cd	Cr	Cu	Fe	Mg	Mn	Ni	Pb	Sb	Se	V	Zn
	(%wt)	(mg/kg)	(mg/kg)	(%wt)	(mg/kg)	(mg/kg)	(mg/kg)	(%wt)	(mg/kg)	(%wt)	(mg/kg)	(%wt)	(mg/kg)	(mg/kg)	(mg/kg)	(mg/kg)
P1	2.84	131	48.8	0.238	1.98	39.2	561	1.62	275	0.767	21.9	19.4	159	2.77	870	110
P2	3.12	153	37.3	0.347	2.55	18.2	431	2.47	330	0.510	18.6	11.3	19.4	2.36	495	90.6
P3	2.67	183	31.3	0.310	2.76	56.8	226	2.46	276	0.715	19.3	11.4	100	3.53	862	73.5
P4	3.96	166	63.3	0.581	3.11	33.5	631	1.05	466	0.575	27.7	16.8	55.5	4.02	869	81.9
P5	1.11	74	28.4	0.245	0.65	53.5	1260	0.736	149	0.798	16.0	12.5	45.7	5.55	1040	119
P6	1.18	76	44.0	0.363	0.86	57.3	906	0.910	264	0.512	10.8	11.0	202	2.78	876	43.6
P7	2.18	117	41.8	0.336	4.44	49.0	337	1.20	290	1.57	31.7	8.34	83.7	10.5	874	127
P8	3.29	128	106	0.490	2.14	19.5	342	2.63	451	0.807	29.1	11.3	11.3	3.86	543	76.1
P9	2.10	99	94.3	0.552	1.50	38.5	237	1.46	373	0.669	21.1	9.80	262	3.77	654	50.4
P10	3.96	157	25.7	0.511	19.22	84.7	642	2.13	823	0.420	21.0	19.0	292	2.43	654	83.5
P11	2.78	149	42.3	0.458	1.53	32.3	416	2.43	520	1.02	37.5	15.3	17.6	6.34	842	76.3
average	2.58	128	53.0	0.427	4.02	47.2	556	1.67	402	0.788	23.8	12.8	119	4.76	802	81.3
max	3.96	183	106	0.581	19.2	84.7	1264	2.63	823	1.57	37.5	19.0	292	10.5	1040	127
min	1.11	73.8	25.7	0.245	0.65	19.5	2260	0.736	149	0.420	10.8	8.34	11.3	2.43	543	43.6
SD	1.05	39.3	29.0	0.118	5.82	19.0	347	0.746	197	0.344	8.35	3.48	106	2.49	154	27.5

variations. This might be caused by different local conditions such as frequency of water use, pipe connection conditions, and the age of the pipe itself. These corrosion products present in the inner walls of the pipes form a surface passivating layer which generally decreases the release of aqueous species of lead to water. However, variations on water quality as result of changes in water treatment can induce chemical transformations that lead to the dissolution of these corrosion products (*3*). For instance, switching disinfectant from chlorine to chloramines resulted high lead levels in drinking water in Washington, DC.and Greensville, NC due to destabilization of the PbO_2 present in the lead scale (*3*). PbO_2 has been reported to be reduced to Pb(II) phases in the presence of natural organic matter or other reductants such as aqueous Mn^{2+} and Fe^{2+} ions (*13, 30*−*32*). The presence of an amorphous phase of lead(IV) oxide in the outermost layer of corrosion scales in our study suggests that moderately chlorinated water (0.5−1 mg Cl_2/L) provides favorable conditions for PbO_2 formation. This observation is consistent with recent reports in the literature (*8, 12*). In addition, we have found that the corrosion scale accumulates other elements such as As, V, Sb, Cu, and Cr. Variations on water quality as result of changes in water treatment can induce chemical transformations that lead to the dissolution of corrosion products. This could result not only in untypically high concentrations of lead in drinking water but could also lead to the release of other toxic elements that were accumulated in the corrosion scale over time.

The chemistry of the corrosion products present in the scale will affect the efficiency of a lead corrosion control

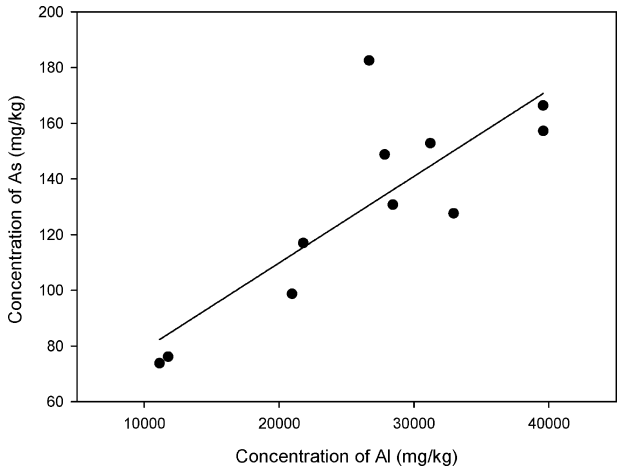

FIGURE 5. Correlation between arsenic and aluminum concentrations.

treatment strategy. Currently, common lead corrosion control methods involve adjustment of pH and alkalinity and addition of corrosion inhibitors such as phosphate and silicate (*14*). Many water utilities including the City of London have increased pH levels to control lead corrosion. While increasing pH can be effective to lower lead concentration because of the relatively low solubility of lead corrosion products at higher pH, this same high pH could promote the dissolution of aluminosilicates (*20*), which can lead to the release of toxic pollutants accumulated in this phase into drinking water. In addition, the high affinity for phosphate displayed by aluminosilicate (*18*) could affect lead corrosion control if an attempt to use phosphates corrosion inhibitors is made. This is even more significant since the outermost part of the corrosion layer is aluminosilicate rich. The comprehensive characterization of corrosion products present in the scale, outlined in this contribution, is essential to predict and model the effects of future changes in water treatment, and to develop an effective corrosion control program.

Acknowledgments

This study has been supported by the Walkerton Clean Water Center and the City of London. We thank John Braam and Dan Huggins, officers of the City of London for their assistance and useful discussions during our study.

Supporting Information Available

Additional tables with London's water quality parameters, Pearson correlations between elements accumulated in the corrosion scales and pictures of the layered lead corrosion scales, XRD, FTIR, and Raman spectra of corrosion scales, and reference materials. This material is available free of charge via the Internet at http://pubs.acs.org.

Literature Cited

(1) Papanikolaou, N. C.; Hatzidaki, E. G.; Belivanis, S.; Tzanakakis, G. N.; Tsatsakis, A. M. Lead toxicity update. A brief review. *Med. Sci. Monit.* **2005**, *11*, RA329–336.

(2) *Lead Control Strategies*; AWWA Research Foundation: Denver, CO, 1990.

(3) Switzer, J. A.; Rajasekharan, V. V.; Boonsalee, S.; Kulp, E. A.; Bohannan, E. W. Evidence that monochloramine disinfectant could lead to elevated Pb levels in drinking water. *Environ. Sci. Technol.* **2006**, *40*, 3384–3387.

(4) Huggins, D. Remediation of lead levels in drinking water: The City of London's experience, *Proceedings of the OWWA/OMWA Joint Annual Conference and Trade Show*, London, ON, April 27−30, 2008.

(5) U.S. Environmental Protection Agency. *Method 3050B Acid Digestion of Sediments, Sludges, And Soils.*: EPA: Washington, DC, 1996.

(6) Frost, R. L.; Fredericks, P. M. Fourier transformation Raman spectroscopy of kandite clays. *Spectrochim. Acta* **1993**, *49A*, 667–674.
(7) Gout, R.; Pokrovski, G. S.; Schott, J.; Zwick, A. Raman spectroscopic study of aluminum silicate complexes at 20°C in basic solutions. *J. Solut. Chem.* **2000**, *29*, 1173–1186.
(8) Aze, S.; Vallet, J.-M.; Pomey, M.; Baronnet, A.; Grauby, O. Red lead darkening in wall paintings: natural ageing of experimental wall paintings versus artificial ageing tests. *Eur. J. Mineral.* **2007**, *19*, 883–890.
(9) Lytle, D. A.; Schock, M. R. Formation of Pb(IV) oxides in chlorinated water. *J. Am. Water Works Assoc.* **2005**, *97* (11), 102–114.
(10) Schock, M. R.; Wagner, I.; Oliphant, R. The corrosion and solubility of lead in drinking water. In *Internal corrosion of water distribution systems, 2nd ed.*; AWWA Research Foundation: Denver, CO, 1996, 131−230.
(11) Dryer, D. J.; Korshin, G. V. Investigation of the reduction of lead dioxide by natural organic matter. *Environ. Sci. Technol.* **2007**, *41*, 5510–5514.
(12) Liu, H.; Korshin, G. V.; Ferguson, J. F. Investigation of the kinetics and mechanisms of the oxidation of cerussite and hydrocerussite by chlorine. *Environ. Sci. Technol.* **2008**, *42*, 3241–3247.
(13) Lin, Y.-P.; Valentine, R. L. Reduction of lead oxide (PbO_2) and release of Pb(II) in mixtures of natural organic matter, free chlorine and monochloramine. *Environ. Sci. Technol.* **2009**, *43*, 3872–3877.
(14) Schock, M. R. Understanding corrosion control strategies for lead. *J. Am. Water Works Assoc.* **1989**, *81*, 88–100.
(15) Mosseri, S.; Henglein, A.; Janata, E. Trivalent lead as a intermediate in the oxidation of Pb^{II} and the reduction of Pb^{IV} species. *J. Phys. Chem.* **1990**, *94*, 2722–2726.
(16) Farmer, V. C.; Fraser, A. R.; Tait, J. M. Characterization of the chemical structures of natural and synthetic aluminosilicate gels and sols by infrared spectroscopy. *Geochim. Cosmochim. Acta* **1979**, *43*, 1417–1420.
(17) Johnson, L. M.; Pinnavaia, T. J. Silylation of a tubular aluminosilicate polymer (imogolite) by reaction with hydrolyzed (γ-aminopropyl) triethoxysilane. *Langmuir* **1990**, *6*, 307–311.
(18) Harsh, J.; Chorover, J.; Nizeyimana, E. *Allophane and Imogolite*, Chapter 9; Soil Science Society of America, Inc.: Madison, WI, 2002.
(19) Opiso, E.; Sato, T.; Yoneda, T. Adsorption and co-precipitation behavior of arsenate, chromate, selenate and boric acid with synthetic allophane-like materials. *J. Hazard. Mater.* **2009**, *170*, 79–86.
(20) Snoeyink, V. L.; Schock, M. R.; Sarin, P.; Wang, L.; Chen, A. S. C.; Harmon, S. M. Aluminum-containing scales in water distribution systems: Prevalence and composition. *J. Water Supply: Res. Technol.* **2003**, *52*, 455–474.
(21) Gustafsson, J. P. Visual MINTEQ. http://www.lwr.kth.se/English/OurSoftware/vminteq/ (accessed July 14, 2010).
(22) He, H.; Barr, T. L.; Klinowsk, J. ESCA and solid-state NMR studies of allophane. *Clay Minerals* **1995**, *30*, 201–209.
(23) Klein, T. M.; Niu, D.; Epling, W. S.; Li, W.; Maher, D. M.; Hobbs, C. C.; Hegde, R. I.; Baumvol, I. J. R.; Parsons, G. N. Evidence of aluminum silicate formation during chemical vapor deposition of amorphous Al_2O_3 thin films on Si(100). *Appl. Phys. Lett.* **1999**, *75*, 4001–4003.
(24) NIST, XPS database. http://srdata.nist.gov (accessed July 14, 2010).
(25) Cooper, M. I.; Fowles, P. S.; Tang, C. C. Analysis of the laser-induced discoloration of lead white pigment. *Appl. Surf. Sci.* **2002**, *201*, 75–84.
(26) Schock, M. R.; Hyland, R. N.; Welch, M. M. Occurrence of contaminant accumulation in lead pipe scales from domestic drinking-water distribution system. *Environ. Sci. Technol.* **2008**, *42*, 4285–4291.
(27) Lytle, D. A.; Sorg, T. J.; Frietch, C. Accumulation of arsenic in drinking water distribution sytems. *Environ. Sci. Technol.* **2004**, *38*, 5365–5372.
(28) Smedley, P. L.; Kinniburgh, D. G. A review of the source, behavior and distribution of arsenic in natural waters. *Appl. Geochem.* **2002**, *17*, 517–568.
(29) Arai, Y.; Sparks, D. L.; Davis, J. A. Arsenate adsorption mechanisms at the allophane-water interface. *Environ. Sci. Technol.* **2005**, *39*, 2537–2544.
(30) Shi, Z.; Stone, A. T. PbO_2 (s, plattnerite) reductive dissolution by natural organic matter: reductant and inhibitory subfractions. *Environ. Sci. Technol.* **2009**, *43*, 3604–3611.
(31) Shi, Z.; Stone, A. T. PbO_2 (s, plattnerite) reductive dissolution by aqueous manganous and ferrous ions. *Environ. Sci. Technol.* **2009**, *43*, 3596–3603.
(32) Liu, H.; Korshin, G. V.; Ferguson, J. F. Interactions of Pb(II)/Pb(IV) solid phases with chlorine and their effects on lead release. *Environ. Sci. Technol.* **2009**, *43*, 3278–3284.

ES101328U